Article

J. Biol. Regul. Homeost. Agents. 2024; 38(6): 4793–4804
https://doi.org/10.23812/j.biol.regul.homeost.agents.20243806.382

Prognostic Value and Immunogenomic Analysis of a Signature Derived from Immune Cell Infiltration in Glioblastoma

Huabin Zhang[1,†], Zhi Li[1,†], Chengxiang Peng[1], Yezhong Wang[1,*], Yunxiang Ji[1,*]

[1]Department of Neurosurgery, Second Affiliated Hospital of Guangzhou Medical University, Guangzhou Medical University, 510261 Guangzhou, Guangdong, China

*Correspondence: wangyezhong@gzhmu.edu.cn (Yezhong Wang); yunxiangji1@126.com (Yunxiang Ji)

[†]These authors contributed equally.

Submitted: 23 January 2024 Revised: 15 February 2024 Accepted: 18 March 2024 Published: 1 June 2024

Background: Glioblastoma (GBM) is the most prevalent primary malignant brain tumor. However, current prognostic indicators do not accurately predict the prognostic and therapeutic benefits of GBM patients, therefore we proposed a new immune-based classification of GBM and find out patients more sensitive to immunotherapy.

Methods: This study established a novel immune-based classification, the immune-related prognostic score (IRPS), by utilizing four GBM cohorts comprising 302 samples. Furthermore, a comprehensive immunogenomic analysis was conducted to assess the relationship between IRPS and clinical prognosis, immune cell infiltration, immune checkpoints, and potential mechanisms of immune evasion. The Chinese Glioma Genome Atlas (CGGA) GBM cohort was also used to validate the IRPS. The findings of this research demonstrate the potential of IRPS as a biomarker for predicting the overall survival (OS) of GBM patients. Additionally, the analysis of Tumor Immune Dysfunction and Exclusion (TIDE) and mRNA stemness index (mRNAsi) has suggested that patients with high IRPS may exhibit increased responsiveness to immunotherapy.

Results: The patients were ranked according to the IRPS score and stratified into high and low IRPS groups. Kaplan-Meier survival analysis revealed a significant difference in prognosis within the two subgroups in both the training and testing datasets. The results showed that the low IRPS subgroup higher degree of immune cell infiltration compared to those of the high IRPS subtype. Tumors in the low IRPS group may express more immune checkpoint molecules as a means of evading immune killing following immune stimulation. In the high IRPS subtype of GBM, *TP53* (49%) was the most frequently mutated gene, while in the low IRPS subtype, only 31% showed this mutation. Moreover, the high IRPS subtype GBM is also more susceptible to mut-p53 therapy degradation compared to GBM of the low IRPS subtype. Additionally, the analysis of TIDE and mRNAsi has suggested that patients with high IRPS may exhibit increased responsiveness to immunotherapy.

Conclusions: These findings suggest that IRPS could function as a reliable prognostic biomarker, facilitate the development of novel immunotherapeutic interventions, and assist in clinical decision-making for GBM patients.

Keywords: glioblastoma (GBM); immune cells; tumor microenvironment; immunotherapy

Introduction

Glioblastoma (GBM) is the prevailing malignant neoplasm of the brain and the most highly aggressive primary tumor within the glioma subcategories, accounting for 54% of all gliomas and 16% of all primary brain tumors [1,2]. Despite advancements in its molecular characterization, the median overall survival rate for patients diagnosed with GBM remains persistently low at 14.6 months [3]. The significance of the tumor microenvironment (TME) in the initiation and progression of cancer has been increasingly recognized [4]. Consequently, understanding the function of the TME can facilitate the development of novel therapies targeting GBM due to its significant contribution to neoplastic progression [5]. Our prior investigation revealed a shift in the composition of tumor-associated myeloid cells towards a greater proportion of monocyte-derived macrophages compared to microglia in recurrent GBM, which correlated with increased invasiveness [6]. Nonetheless, current clinical practice fails to assess tumor-infiltrating immune cells (TIICs) in GBM, resulting in limited accuracy in prognosis and therapy response prediction. Therefore, computational methods provide a viable alternative to quantify a large number of TIICs, offering a more comprehensive understanding of the interplay between prognosis and TIICs in GBM.

The current study aimed to develop an immune-related prognostic score (IRPS) for GBM by investigating the relationship between the activity profile of TIICs and the overall survival of GBM patients. To achieve this, GBM training cohorts from four publicly available databases were

Journal of
BIOLOGICAL REGULATORS
and Homeostatic Agents

used to employ the Least Absolute Shrinkage and Selection Operator (LASSO) and Cox model, which identified 36 immune cell signatures significantly correlated with survival. Subsequently, an IRPS for GBM was created utilizing these prognostic-related immune cell types, and it was correlated with GBM patients' overall survival time and immunophenotypic profiles. An integrated analysis approach was employed to examine the differences in genome, TME, and immunogenomic profiles between low and high IRPS patients. This study aimed to improve personalized survival prognosis and treatment alternatives for physicians and glioblastoma patients by identifying the diverse advantages of immunotherapy and chemotherapy using an innovative classification system based on immune cells.

Materials and Methods

Preprocessing of Cohort Datasets

The mRNA expression data and copy number variants of patients with glioblastoma were obtained from the UCSC Xena The Cancer Genome Atlas (TCGA) GBM cohort (https://xenabrowser.net/). The relevant clinical data for TCGA-GBM samples were obtained using the cgdsr R package from the cBioPortal [7]. The mutation profiling was obtained from the TCGA data portal (https://portal.gdc.cancer.gov/) using the TCGAbiolinks (https://github.com/BioinformaticsFMRP/TCGAbiolinks) R package [8]. The study acquired gene expression profiles from three distinct datasets via the GBM Gene Expression Omnibus (GEO) database. Additionally, the Chinese Glioma Genome Atlas (CGGA)-GBM cohort (testing dataset) provided IlluminaHiSeq RNA-seq data and clinical information for 139 glioblastoma patients, obtained from the CGGA database. **Supplementary Fig. 1** presents the specific collection data, while **Supplementary Table 1** describes the clinical data for these cohorts. The cohorts included in the study were limited to those with a sample size of over 50 GBM and with available overall survival data. To ensure uniformity in data processing, the combat function from the sva (https://bioconductor.org/packages/release/bioc/html/sva.html) R package [9] was utilized to adjust for batch effects in the TCGA, CGGA, and GEO datasets.

Gene Set Enrichment Analysis

A comprehensive literature search was conducted to gather 98 immune cell signatures for evaluating the infiltration of immune cells in tumors [10–17]. The single sample gene set enrichment analysis (ssGSEA) package within the GSVA (https://bioconductor.org/packages/release/bioc/html/GSVA.html) R package [18] was utilized to calculate a Normalized Enrichment Score (NES) for these signatures in the tumor microenvironment.

The Immune-Related Prognostic Score (IRPS) of GBM

The NES was employed to evaluate the degree of TICs signatures in all patients through ssGSEA. Univariate Cox proportional hazards regression analyses were conducted to evaluate the association between NES scores and overall survival (OS) in a cohort of 302 GBM patients (training datasets). Immune-cell signatures with $p < 0.05$ were filtered. Hazard ratios (HR) were employed to identify immune cell signatures that provide protection (HR <1) or pose a risk (HR >1). Ultimately, a prognostic signature named IRPS for GBM samples, using the scores of 4 GBM datasets and 35 immune cell signatures, was described as: IRPS = ΣNES (HR <1) – ΣNES (HR >1).

Immune Infiltration and Immunotherapy Response Prediction

Each GBM sample was estimated using the Estimation of STromal and Immune cells in MAlignant Tumor tissues using Expression data (ESTIMATE) (Version 2.0.0, MD Anderson, Houston, TX, USA) R package with default parameters [19]. To determine the ratio of 22 subtypes of TICs in GBM mass, the CIBERSORT (Version 1.03, the Alizadeh Lab and Newman Lab, Stanford, CA, USA) website was employed [12]. Furthermore, 11 of the 98 immune cell signatures were excluded from the analysis due to containing less than 10 genes. Ultimately, 87 immune cell signatures were utilized in the final analysis. The NES produced by gene set enrichment analysis (GSEA) was regarded as the degree of infiltration for each immune cell signature.

The Tumor Immune Dysfunction and Exclusion (TIDE) algorithm was utilized to predict the individual's probability of reacting to immunotherapy, specifically the blocking of immune checkpoints [20]. Furthermore, a machine learning algorithm was previously reported to calculate stem-like indices for TCGA-GBM samples [21].

Differential Gene Expression and Functional Enrichment Analysis

The R package Limma (https://bioconductor.org/packages/release/bioc/html/limma.html) was utilized for conducting differential expression analysis [22]. Differential genes were identified based on a threshold of p.adj < 0.05 and a fold change >2 or fold change <0.5. Additionally, the package clusterProfiler was employed to analyze Gene Ontology (GO) and Kyoto Encyclopedia of Genes and Genomes (KEGG) functional enrichment (https://bioconductor.org/packages/release/bioc/html/clusterProfiler.html) [23].

Copy Number Variations (CNV) Analysis

This study employed the Genomic Identification of Significant Targets in Cancer (GISTIC) algorithm to identify common regions of copy number alteration across all samples [24]. The default parameters of GISTIC were uti-

lized, with a significance threshold of Q <0.05 and a confidence level of 0.95 to determine the peak interval. The GISTIC analysis was performed using the MutSigCV module of GenePattern (https://cloud.genepattern.org). Furthermore, the somatic mutation data for all samples were analyzed using the maftools (https://bioconductor.org/packages/release/bioc/html/maftools.html) R package [25].

Statistical Analysis

Survival curves were calculated using the Kaplan-Meier methodology, and differences were compared using the Log-rank test integrated into the survival package for R (https://github.com/therneau/survival). The R package "pROC" was used to compute the receiver operating characteristics curve [26].

All statistical analyses to determine the relation between features and patient outcomes were performed using R (Version 3.5.0, Bell Laboratories, Boston, MA, USA). The statistical significance was determined by both-sided *p*-values, with a significance level set at $p < 0.05$.

Results

IRPS Building and the Relation with Immune-Cell Signatures

The workflow design of this study is illustrated in **Supplementary Fig. 2A**. This study aimed to develop a prognostic model for GBM patients by analyzing a compendium of 98 immune cell types that infiltrated tumors. As shown in Fig. 1A, NES through ssGSEA was used to assess the level of immune infiltration in each sample. Subsequently, univariate Cox proportional hazards regression analysis was employed to determine the association between the NESs and OS of 302 GBM patients. The findings are presented in **Supplementary Table 2 ssGSEA**. In this study, 35 immune cell signatures with a *p*-value less than 0.05 were selected. The immune, stromal, and ESTIMATE scores, as well as tumor purity of the samples, were evaluated using the R package estimate. The results showed that the low IRPS subgroup had higher immune, stromal, and ESTIMATE scores, and lower tumor purity (Fig. 1A, **Supplementary Table 2 estimate score**). Additionally, a forest plot in **Supplementary Fig. 2B** demonstrated the associations between each immune cell subset and OS in the training cohort. The IRPS scoring system was applied to the mRNA expression profile from the training and testing datasets to determine the IRPS values for all samples. The IRPS for each sample is shown in **Supplementary Table 2 IRPS** and **Supplementary Table 3 IRPS CGGA**. Subsequently, patients were divided into two subgroups by using the cutoff IRPS value. Statistical analysis revealed a significant difference in prognosis within the two subgroups in both the training and testing datasets (Fig. 1B,C). To assess the reliability of the IRPS risk model, Receiver Operating Characteristic (ROC) curves were used, yielding an Area under curve (AUC) of 0.54, 0.73, and 0.72 for 1-year, 3-year, and 5-year predictions in the testing set, respectively (Fig. 1D). These findings suggest that the IRPS risk model has the potential to predict the prognosis of GBM patients in the testing dataset.

Correlation between IRPS and TIME Patterns

To assess the immune infiltration in tumors, the ESTIMATE algorithm, GSEA, and CIBERSORT formula were used to investigate the variation in TIICs within high and low IRPS subtypes. The ESTIMATE algorithm was utilized to calculate the ESTIMATE, immune, stromal, and tumor purity scores in GBM tissues. The results indicated a negative correlation between IRPS and the Immune ($R = –0.93$, $p < 2.2^{-16}$), Stromal ($R = –0.9$, $p < 2.2^{-16}$), and ESTIMATE scores ($R = –0.95$, $p < 2.2^{-16}$) (Fig. 2A–C). This suggests that tumors of the low IRPS subtype exhibit a higher degree of immune cell infiltration compared to those of the high IRPS subtype. In contrast, a strong positive correlation was observed between the IRPS and tumor purity ($R = 0.95$, $p < 2.2^{-16}$), as depicted in Fig. 2D. Low tumor purity has been associated with a poor prognosis in glioma, as previously reported [24]. These findings were further validated in the testing dataset (**Supplementary Fig. 3A**).

The volcano plots and enrichment plots from the GSEA analysis revealed distinct patterns of immune infiltrates between the two subtypes, as demonstrated in Fig. 2E,F, and **Supplementary Table 4 gsea**. Notably, several immune cell types exhibited significantly high infiltration when comparing the low IRPS subtype to its high counterparts, such as MacTh1 cluster, Macrophages, Monocyte, Myeloid-Derived Suppressor Cell (MDSC), and T cells gamma delta.

Results of the CIBERSORT algorithm were used to analyze the results of two IRPS subtypes. In the low IRPS subtype, there was a significant increase in T cell subsets, including T cell $CD4^+$ memory resting, T cell $CD4^+$ naïve, T cell $CD8^+$ and T cell regulatory. Meanwhile, in the low IRPS group, there was a significant increase in M2 macrophages and monocytes (Fig. 2G,H). Similar findings were observed in the testing set (**Supplementary Fig. 3B**).

IRPS and Intrinsic Immune Escape Mechanism in GBM

A further investigation was conducted on the relationship between the IRPS and intrinsic immune escape mechanisms. Tumor cells exhibiting intrinsic immune escape are believed to control their immune evasion. A previous study identified cancer immunogenicity and immune-checkpoint molecule expression as contributing factors to intrinsic immune escape [25].

Several factors, including neoantigen load, chromosomal instability levels, mutation load, and Homologous Recombination Deficient (HRD), can influence tumor immunogenicity. It was observed that the level of HRD was

Journal of
BIOLOGICAL REGULATORS
and Homeostatic Agents

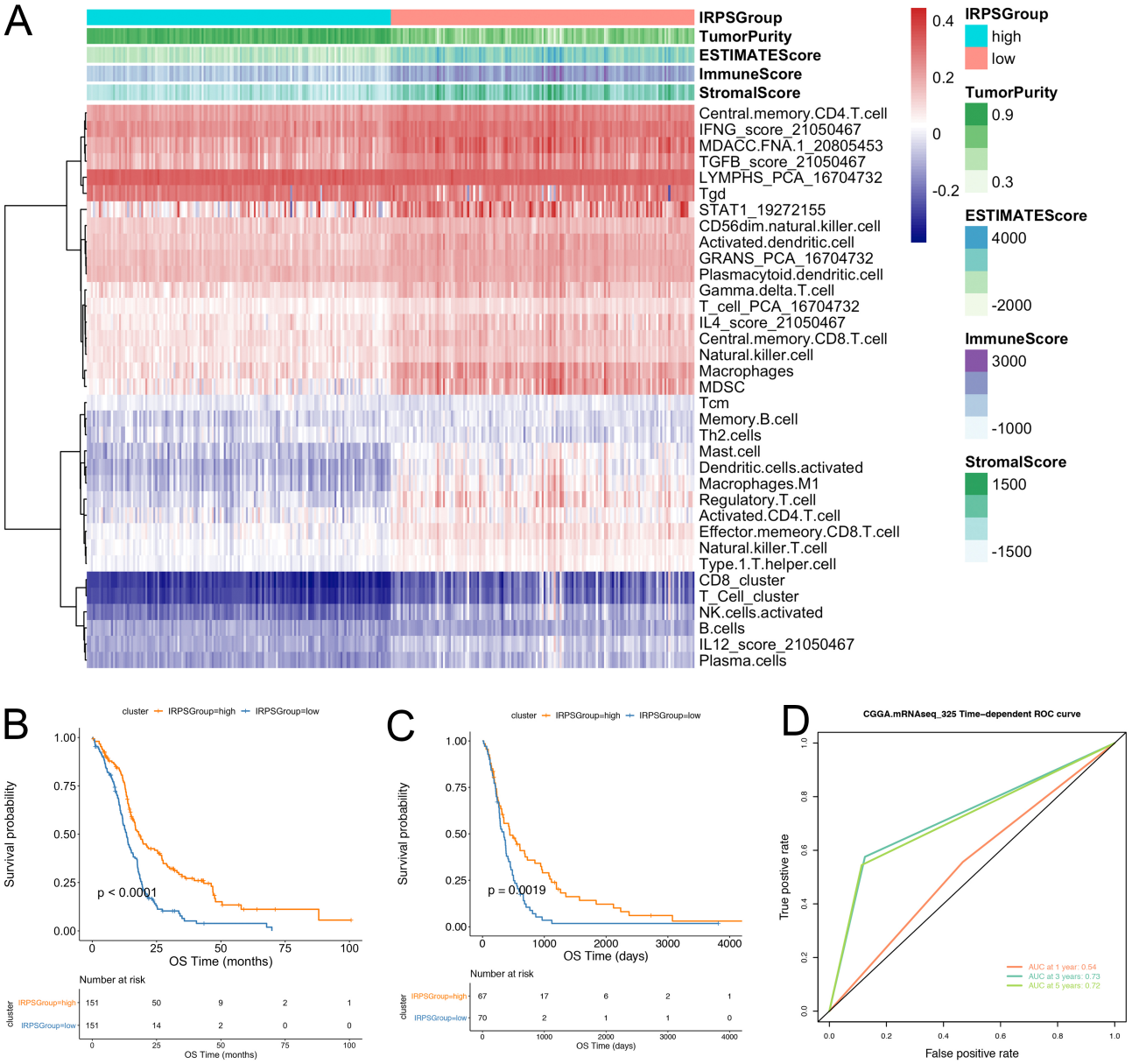

Fig. 1. IRPS scores were correlated with the survival of GBM patients. (A) GBM patients were categorized into 2 subgroups (high and low IRPS) based on ssGSEA immune signatures. (B) GBM Kaplan-Meier curve according to IRPS subtypes (training dataset) patients. (C) GBM Kaplan-Meier curve according to IRPS subtypes (testing dataset) patients. (D) The 1-year, 3-year and 5-year ROC curves for the CGGA dataset. GBM, glioblastoma; IRPS, immune-related prognostic score; CGGA, Chinese Glioma Genome Atlas; ROC, Receiver Operating Characteristic; ESTIMATE, Estimation of STromal and Immune cells in MAlignant Tumor tissues using Expression data; IFNG, Interferon Gamma; MDACC, M.D. Anderson Cancer Center; FNA, Fine-needle Aspiration; TGFB, Transforming Growth Factor-beta; LYMPHS, Lymphocytes; PCA, Prostatic Cancer; STAT1, Signal Transducer and Activator of Transcription 1; GRANS, Granulocytes; IL, Interleukin; MDSC, Myeloid-Derived Suppressor Cell; OS, overall survival; ssGSEA, single sample gene set enrichment analysis; AUC, Area under curve.

significantly increased in the high IRPS subtype compared to the low IRPS subtype (Fig. 3A). Moreover, a positive correlation (R = 0.28, p = 0.0093) was observed between HRD and IRPS (Fig. 3B). However, the mean values of Neoantigen (Single Nucleotide Variant (SNV) and Indel), Copy Number Aberration (CNA)-frac-altered (chromosomal instability level), and mutation load (silent and non-silent) did not exhibit any significant difference between the low and high IRPS subtypes, as demonstrated in Fig. 3A. Additionally, the TCGA-GBM cohort did not reveal any significant correlation between neoantigen load, chromosomal instability levels, and mutation load with the IRPS index, as illustrated in Fig. 3B and **Supplementary Table 5 publicinfor**.

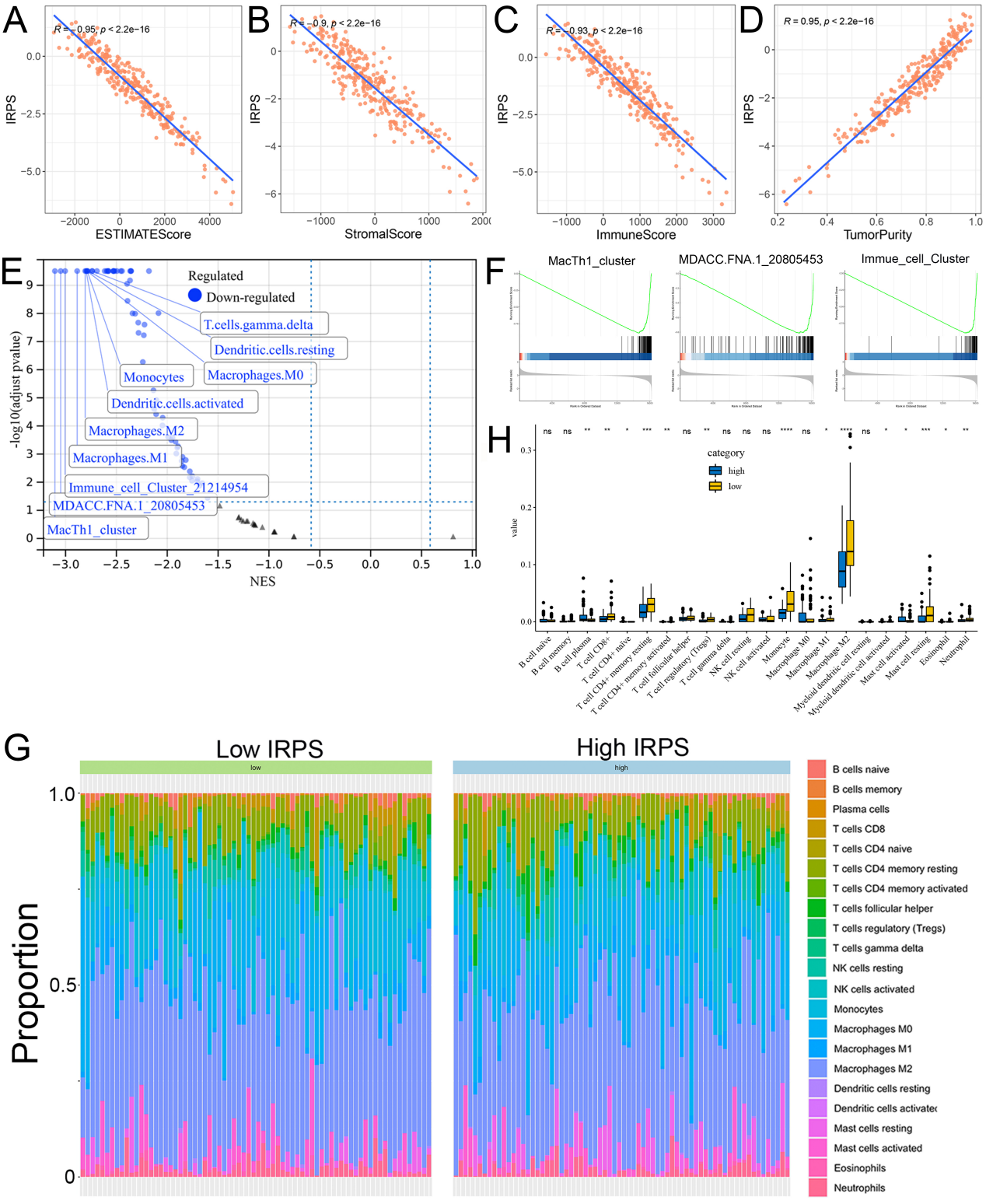

Fig. 2. Immune microenvironment profiles and immunogenomic characteristics of GBM in relation to IRPS. Analyses of correlations between IRPS and (A) ESTIMATE scores, (B) stromal scores, (C) immune scores, and (D) tumor purity. (E) A volcano plot comparing patients with high IRPS subtypes to patients with low IRPS subtypes in the training dataset. (F) GSEA of MacTh1 cluster, MDACC.FNA1.1 20805453, and Immune cell cluster 21214954 comparisons between patients with a high IRPS subtype and patients with a low IRPS subtype was conducted for the training dataset. (G,H) Proportion and comparisons of the abundances of 22 immune cells in two subtypes by CIBERSORT. (*$p < 0.05$; **$p < 0.01$; ***$p < 0.001$; ****$p < 0.0001$; ns, $p > 0.05$). NES, Normalized Enrichment Score; GSEA, gene set enrichment analysis.

Journal of
BIOLOGICAL REGULATORS
and Homeostatic Agents

The expression of immune checkpoints was identified as another crucial intrinsic immune escape mechanism. An in-depth analysis of the expressions of six immune checkpoints in the training and validation datasets revealed that the expression levels of programmed cell death protein (PD)-1, PD-L1, Cytotoxic T-lymphocyte-Associated Protein (CTLA)-4, T cell Immunoglobulin and Mucin-containing-molecule (TIM)-3, and T cell immunoreceptor with Immunoglobulin and ITIM domain (TIGIT) were significantly higher in the low IRPS subtype compared to the high IRPS subtype in both datasets. Additionally, Lymphocyte Activation Gene (*LAG*)-*3* showed no statistical difference between both subtypes of GBM in the training and testing datasets (Fig. 3C and **Supplementary Fig. 4A**). These results suggest that tumors in the low IRPS group may express more immune checkpoint molecules as a means of evading immune killing following immune stimulation. Furthermore, a comprehensive analysis was conducted to examine the correlation between clinical parameters and IRPS, as presented in **Supplementary Table 6 cliniinfor** and **Supplementary Fig. 4B**, which revealed that patients with *IDH1* mutations exhibited higher IRPS levels.

Correlations between IRPS and Genomic Variables in TCGA-GBM

Genomic alterations, such as mutations and copy number variations (CNVs), can significantly impact tumor immunity. Therefore, we conducted a comprehensive analysis of CNVs and somatic mutations across various stemness subtypes. The top mutated genes in the low and high IRPS subtypes are presented in Fig. 4A,B. In the high IRPS subtype of GBM, *TP53* (49%) was the most frequently mutated gene, while in the low IRPS subtype, only 31% showed this mutation. On the other hand, *TTN* (41%) was the most frequently mutated gene in the low IRPS subtype, with only 30% mutation in the high IRPS subtype. Another notable mutated gene was phosphatase and tensin homolog (*PTEN*), with a mutation frequency of 40% in the low IRPS subtype and 29% in the high IRPS subtype. In addition, the GISTIC analysis identified chromosome 12q14.1, including the Cyclin-dependent kinase (CDK) 4 locus, as a significantly amplified site in the high IRPS subtype compared to the low IRPS subtype GBM (Fig. 4C,D).

We investigated the varying sensitivity of different IRPS subtypes to TP53-targeted therapy due to significant differences in *TP53* mutation. TP53-targeted therapy for tumors primarily involves degrading mut-p53 and restoring wt-p53 [25]. For instance, vorinostat, an HDAC inhibitor, can degrade mut-p53 and reduce GBM stem cell viability [26]. We assessed the response to vorinostat in the two IRPS subtypes using the pRRophetic R package, which relies on data from the GDSC (Version 8.5, Wellcome, Boston, MA, USA) database. The 50% inhibiting concentration (IC_{50}) of vorinostat showed a significant reduction in the high IRPS subtype as anticipated ($p = 0.0017$) (Fig. 4E). This suggests that GBM of the high IRPS subtype is more susceptible to mut-p53 therapy degradation compared to GBM of the low IRPS subtype. Nutlin-3a can increase wt-p53 expression both *in vitro* and *in vivo* in GBM by inhibiting MDM2 [27]. Fig. 4F shows that the IC_{50} of nutlin-3a in GBM patients was significantly lower in the low IRPS subtype GBM compared with the high IRPS subtype ($p = 0.0358$). Since CDK4 is highly amplified in the high IRPS subtype GBM, the IC_{50} of palbociclib (CDK 4 inhibitor) was also evaluated and found to be significantly lower in the high IRPS subtype GBM ($p = 0.0316$) (Fig. 4G). Furthermore, Temozolomide (TMZ) treatment has been established as the conventional chemotherapy for GBM following surgical intervention. Consequently, we assessed the response to TMZ in the two distinct subtypes of IRPS. However, the estimated IC_{50} values of TMZ showed no difference between the two IRPS subtypes ($p = 0.313$) (Fig. 4H).

Differential Expression and Functional Enrichment Analysis between High and Low IRPS Subtypes

We conducted a differential expression analysis to compare the gene expression profiles of the high and low IRPS subtypes. A comprehensive analysis revealed the identification of 267 differentially expressed genes (DEGs) ($|\log2FC| > 1.0$) in the low IRPS subtype, consisting of 41 upregulated genes and 226 downregulated genes (Fig. 5A,B, **Supplementary Table 7 diffgene**). Subsequently, we performed functional enrichment analysis using WebGestaltR. A total of 520 Biological Processes (BPs) were found to be significantly enriched ($p < 0.001$), which included leukocyte migration, neutrophil activation, and neutrophil-mediated immunity. Additionally, 78 Cellular Components (CCs) were significantly enriched, such as the Major Histocompatibility Complex (MHC) class II protein complex and immunoglobulin complex. Furthermore, 75 Molecular Functions (MFs) were significantly enriched, including antigen binding, immune receptor activity, and cytokine activity. Lastly, 54 KEGG pathways were significantly enriched, such as the focal adhesion, antigen processing and presentation, and the Toll-like receptor signaling pathway (Fig. 5C–F, **Supplementary Table 7**).

The IRPS could Predict the Therapeutic Benefit

Previous research utilizing machine learning techniques has suggested that TIDE and mRNA stemness index (mRNAsi) are effective tools for predicting the response to immunotherapy in patients with GBM [19]. In this study, the TIDE and mRNAsi algorithms were employed to forecast the probability of immunotherapy responses. The results, depicted in Fig. 6A–D, indicate that GBM patients with a low IRPS subtype exhibit elevated TIDE and reduced mRNAsi in both the training and testing datasets (**Supplementary Table 8 mRNAsi** and **Supplementary Table 9 TIDE**). These findings are consistent with previ-

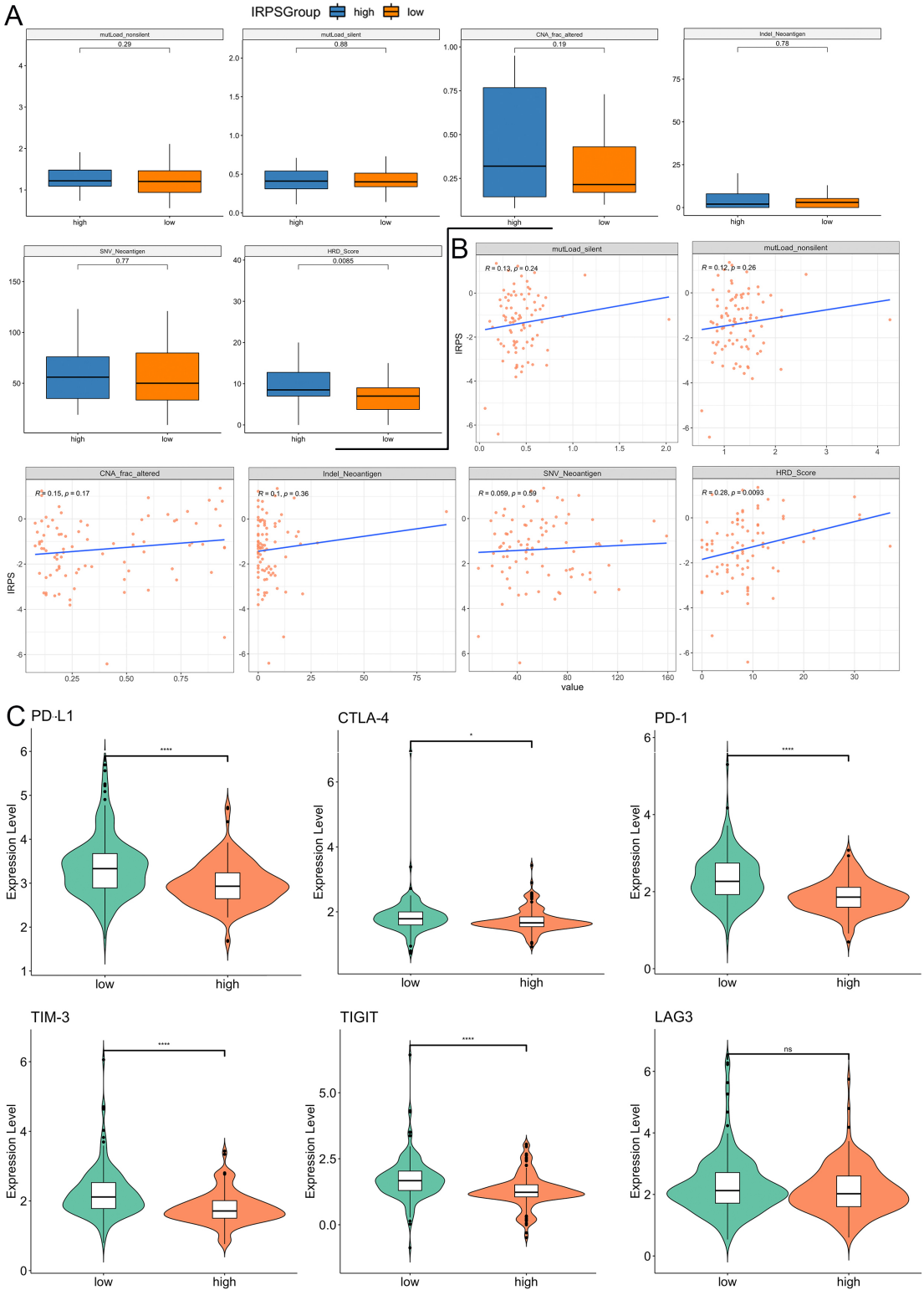

Fig. 3. IRPS and intrinsic immune escape mechanism in GBM. (A) The comparison of mutLoad nonsilent, mutLoad silent, CNA frac altered, Indel Neoantigen, SNV Neoantigen, and HRD score between low and high IRPS subtypes in GBM patients. (B) The correlation between IRPS and mutLoad nonsilent, mutLoad silent, CNA frac altered, Indel Neoantigen, HRD score, SNV Neoantigen. (C) The association between IRPS and immune checkpoints in the training dataset. (*$p < 0.05$; ****$p < 0.0001$; ns, $p > 0.05$). HRD, Homologous Recombination Deficient; SNV, Single Nucleotide Variant; CNA, Copy Number Aberration; PD, programmed cell death protein; CTLA, Cytotoxic T-lymphocyte-Associated Protein; TIM, T cell Immunoglobulin and Mucin-containing-molecule; TIGIT, T cell immunoreceptor with Immunoglobulin and ITIM domain; *LAG*, Lymphocyte Activation Gene.

Journal of
BIOLOGICAL REGULATORS
and Homeostatic Agents

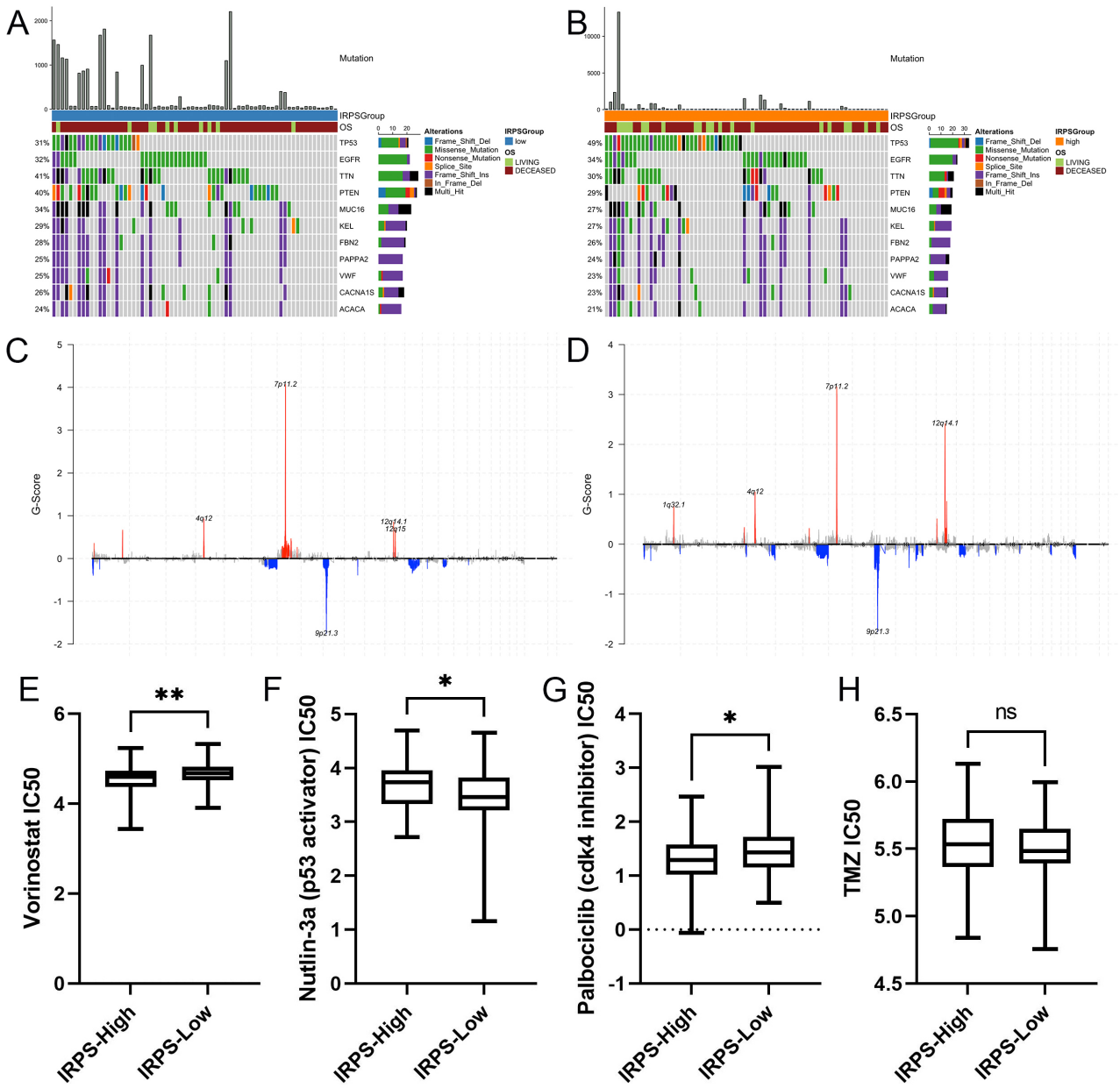

Fig. 4. Correlations between IRPS and genomic variables in TCGA-GBM. (A) Waterfall plots showing the most frequently mutated genes in the low IRPS subtype of GBM. (B) Waterfall plots showing the most frequently mutated genes in the high IRPS subtype of GBM. (C) Genomic Identification of Significant Targets in Cancer (GISTIC) analysis of copy-number changes in the low IRPS subtype of GBM. (D) GISTIC analysis of copy-number changes in the high IRPS subtype of GBM. The IC_{50} differences of (E) vorinostat, (F) nutlin-3a, (G) palbociclib, and (H) Temozolomide (TMZ) predicted by the pRRophetic algorithm between high-/low- IRPS subtypes (*$p < 0.05$; **$p < 0.01$; ns, $p > 0.05$). TCGA, The Cancer Genome Atlas; IC_{50}, 50% inhibiting concentration.

ous investigations, which have shown that high TIDE and low mRNAsi levels are indicative of greater sensitivity to immunotherapy [19]. Consequently, these findings suggest that patients with high IRPS subtype GBM are more likely to be more sensitive to immunotherapy.

This study investigated the prognostic significance of the IRPS in a group of GBM samples that underwent chemotherapy, specifically Gene Expression Omnibus Series (GSE) 17227 and GSE140145. Notably, the GSE17227 dataset showed a statistically significant decrease in IRPS values in GBM samples that were treated with all-trans retinoic acid (ATRA) compared to their pretreatment levels (Fig. 6E). Furthermore, the training dataset enabled the estimation of the IC_{50} of ATRA in two subtypes. The IC_{50} of ATRA was significantly reduced in patients with a high IRPS ($p = 0.0024$) (Fig. 6F). The GSE140145 dataset sam-

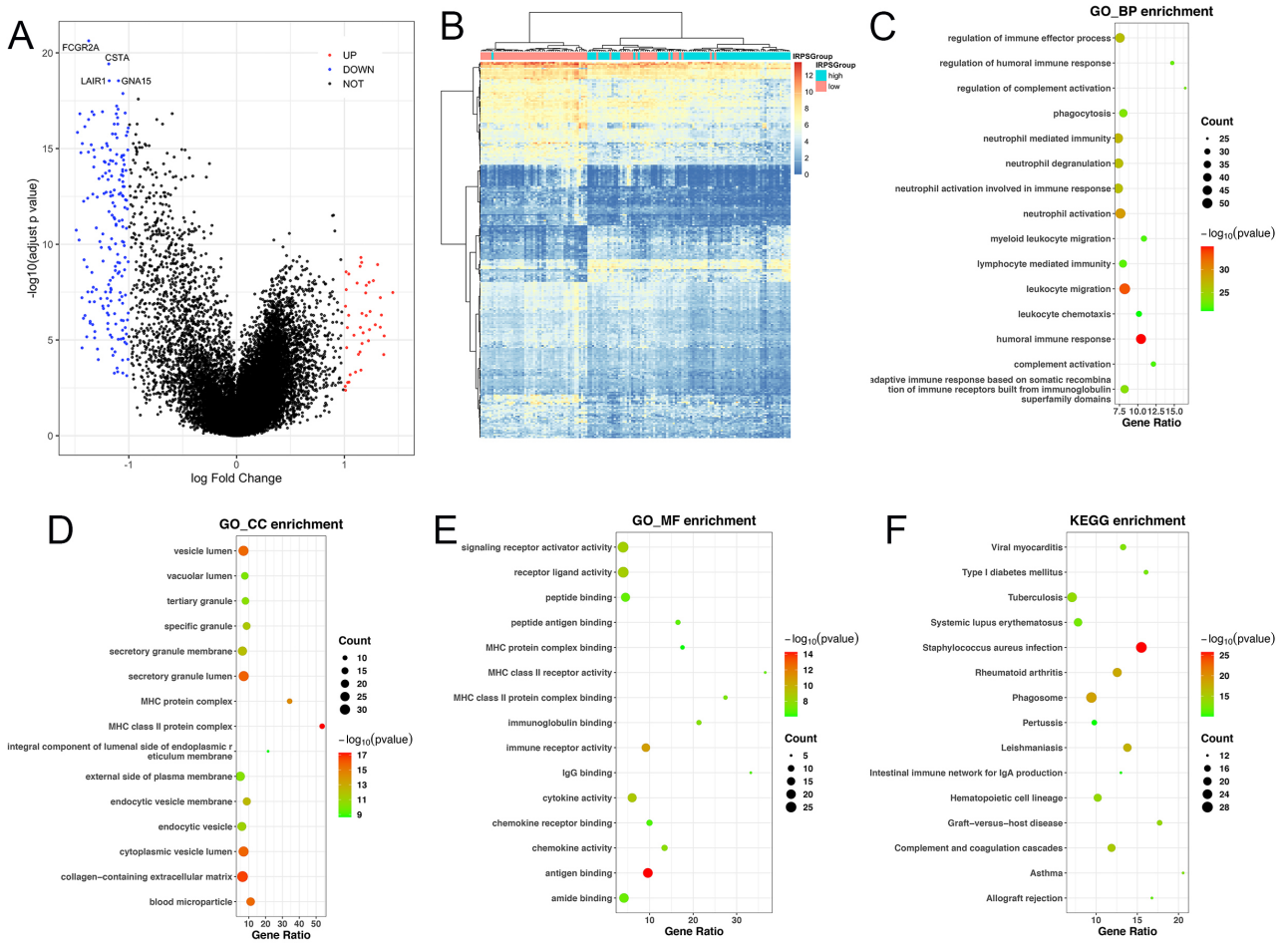

Fig. 5. Identification of two subtypes with distinct gene expressions and functional annotations. (A) Volcano plot and (B) heatmap showing the expression profiles between low and high IRPS subtypes. Differentially expressed genes (DEGs) functional enrichment analysis, encompasses significant enrichment in (C) biological processes, (D) cellular components, (E) molecular functions and (F) Kyoto Encyclopedia of Genes and Genomes (KEGG) pathways. GO, Gene Ontology; BP, Biological Processe; MF, Molecular Function; CC, Cellular Component; MHC, Major Histocompatibility Complex.

ples were treated with alectinib, an anaplastic lymphoma kinase (ALK) inhibitor. Subsequent analysis showed no significant change in IRPS (Fig. 6G). In two subtypes of the training dataset patients, the IC_{50} values of crizotinib, another ALK inhibitor, were calculated and no significant difference was found between the estimated values (Fig. 6H). The IRPS value was identified as a predictive biomarker for chemotherapeutic benefits, demonstrating its predictive power.

Discussion

In this study, the relationship between GBM TIICs and immunotherapy and chemotherapy was analyzed. A method was proposed to divide subtypes based on TIICs, developing an approach for distinguishing subtypes based on TIICs and validating their classification through the examination of patient samples and clinical data obtained from the TCGA, CGGA, and various GEO cohorts. The IRPS model was based on 35 immune cells, of which 31 showed a negative correlation with overall survival time, while the remaining four displayed positive correlations with overall survival time. The prognostic value of the IRPS model was confirmed in the TCGA cohort, CGGA cohort, and several GEO cohorts. The survival curves differed significantly, indicating the good prognostic power of the IRPS model.

The central nervous system's relative immunological privilege has led to extensive research into immunotherapy for GBM patients in recent years, encompassing cellular immunotherapy, antitumor vaccines, and immune checkpoint inhibitors [27]. However, the outcomes of phase III clinical trials for GBM have been unsatisfactory compared to other tumors. Therefore, identifying patients who may benefit from immunotherapy in precision treatment is a crucial step. In this study, we utilized TIDE and mRNAsi methodologies to verify the immunotherapy response in low- and high-IRPS subtypes of GBM. Jiang *et*

Journal of
BIOLOGICAL REGULATORS
and Homeostatic Agents

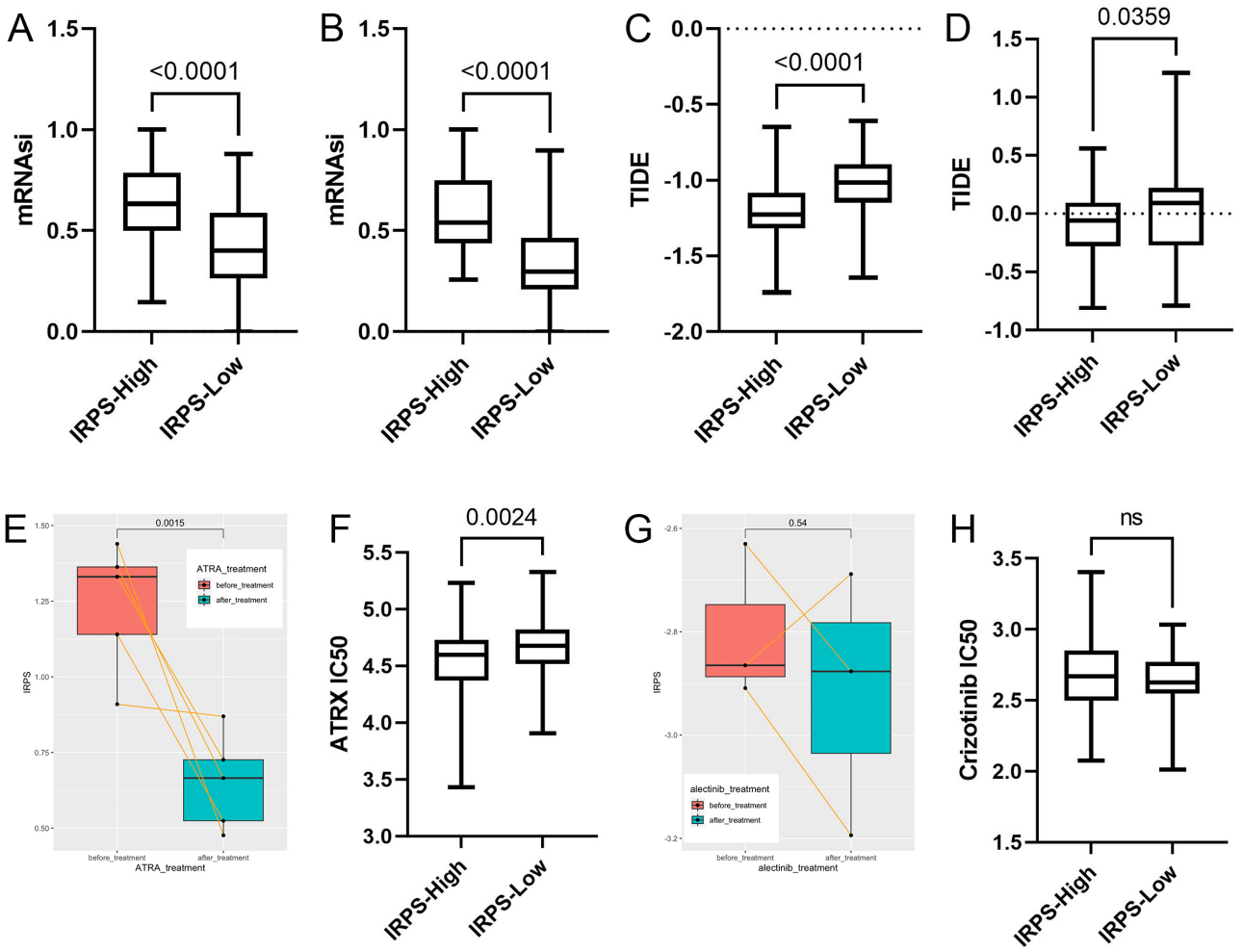

Fig. 6. The therapeutic benefit of the IRPS value. (A) Boxplot showing the stemness index between two IRPS subtypes in the training dataset. (B) Boxplot showing the stemness index between two IRPS subtypes in the testing dataset. The comparison of Tumor Immune Dysfunction and Exclusion (TIDE) between two IRPS subtypes in (C) the training dataset and (D) the testing dataset. (E) Pairwise comparison of the IRPS in patients before and after all-trans retinoic acid (ATRA) treatment. (F) The IC_{50} differences of ATRA predicted by the pRRophetic algorithm between high-/low- IRPS subtypes. (G) Pairwise comparison of the IRPS in patients before- and after alectinib treatment. (H) The IC_{50} differences of crizotinib predicted by the pRRophetic algorithm between high-/low- IRPS subtypes. (ns, $p > 0.05$). ATRX, All-Trans Retinoic Acid; mRNAsi, mRNA stemness index.

al. [20] discovered that the TIDE algorithm can be employed to anticipate the immunotherapeutic response by analyzing the mRNA expression of GBM tissues. Yang *et al*. [28] found that GBM patients with elevated TIDE scores are more prone to anti-tumor immune evasion. Additionally, some studies have suggested that GBM patients with high mRNAsi scores may experience a more favorable response to immunotherapy [21,29]. Our results showed that high-IRPS patients with lower TIDE and higher mRNAsi scores may benefit more from immunotherapy treatment in the context of GBM. Furthermore, patients with GBM harboring a *PTEN* mutation exhibit a reduced response rate to anti-PD-1 immunotherapy, which can be attributed to the mutation-induced alterations in the immune microenvironment. Additionally, a higher prevalence of *PTEN* mutations was observed in the low-IRPS group within the TCGA-GBM cohort. Notably, *PTEN* mutation ranks as the most impactful mutation gene in GBM, significantly reducing survival rates. These findings partially explain the efficacy of IRPS in predicting the outcomes and immunotherapeutic responsiveness of GBM patients.

Chemotherapy is currently a primary approach for managing GBM patients, emphasizing the importance of identifying predictive markers for chemotherapy in GBM treatment. The role of DNA repair, particularly HRD, is pivotal in cancer chemotherapy susceptibility. The findings of our study indicate a significant positive correlation between the HRD score and IRPS score in GBM patients. HRD has previously been associated with increased sensitivity to chemotherapy and longer overall survival [30]. Additionally, a prior study showed that the absence of *TP53* expression enhances the susceptibility of glioblastoma to

supplementary chemotherapeutic agents and diminishes the likelihood of resistance to TMZ [31]. Consistent with this research, our study revealed a higher incidence of *TP53* mutations in the high-IRPS group (49%) compared to the low-IRPS group (31%). For further verification of the clinical implementation of the IRPS, two cohorts of GBM patients with available chemotherapy data were obtained from the GEO database, and IRPS scores were computed for both cohorts. Examination of these GBM datasets revealed that patients treated with sensitive chemotherapy showed a significant change in their IRPS, whereas those treated with insensitive chemotherapeutics exhibited a nonsignificant response. This suggests that the IRPS model could be a sensitive indicator of chemotherapeutics for GBM treatment.

This study had certain limitations. Specifically, although it has been established that the impact of chemotherapy and immunotherapy depends on tumor heterogeneity, our investigation did not account for the intratumorally or interpatient heterogeneity of the GBM immune microenvironment. Furthermore, while the GBM cohorts have shown the survival advantages of certain infiltration cells, the underlying mechanisms of these cells remain unclear. Therefore, further experimental research is necessary to elucidate the functional roles of these immune cell types in GBM and provide crucial insights for a more comprehensive understanding of the disease. Thirdly, the classification of GBM cancer samples into high and low IRPS subtypes was based solely on the median cutoff of IRPS. However, to improve the stratification of GBM patients, it may be necessary to determine the optimal cutoff of IRPS. Finally, the IRPS utilized immune cells, with significant correlations found with overall survival time. However, the study exhibited a deficiency in providing precise details regarding immune-related genes that displayed a significant correlation with the overall survival duration within distinct immune cell types.

The IRPS has proven to be a significant indicator due to its correlation with immune infiltrate levels and its association with overall survival across a comprehensive range of GBM cohorts, establishing it as a potent prognostic marker for GBM. The IRPS is poised to enhance the prognostic accuracy of GBM patients, enable comparative analysis of immune modulators, and facilitate the identification of GBM patients who are likely to benefit from immunotherapy and chemotherapy.

Conclusions

In conclusion, the potential of immunotherapy and chemotherapy in treating GBM remains significant, and the identification of patients who are likely to benefit from these treatments is a crucial task. This study aimed to classify patients into distinct subtypes based on GBM immune cell infiltration and predict their response to immunotherapy and chemotherapy, thereby offering a potential strategy for patient screening. The utilization of the IRPS model has the potential to establish a prognosis for patients with GBM and to categorize those who may derive therapeutic benefits from chemotherapy and anticancer immunotherapy.

Availability of Data and Materials

The codes and dataset used analyzed during the this study are available from the corresponding authors on reasonable request.

Author Contributions

YJ and YW designed the research study. HZ and ZL performed the research. HZ, ZL and CP analyzed the data. YW and YJ jointly supervised this work. All authors contributed to editorial changes in the manuscript. All authors read and approved the final manuscript. All authors have participated sufficiently in the work and agreed to be accountable for all aspects of the work.

Ethics Approval and Consent to Participate

Not applicable.

Acknowledgment

We are grateful to the TCGA and CGGA projects as well as the staff and patients in the projects.

Funding

Funding for this study was provided by the Science and Technology Plan of Guangzhou City Health Commission (no: 20211A010058).

Conflict of Interest

The authors declare no conflict of interest.

Supplementary Material

Supplementary material associated with this article can be found, in the online version, at https://doi.org/10.23812/j.biol.regul.homeost.agents.20243806.382.

References

[1] Malzkorn B, Reifenberger G. Practical implications of integrated glioma classification according to the World Health Organization classification of tumors of the central nervous system 2016. Current Opinion in Oncology. 2016; 28: 494–501.

[2] Ostrom QT, Gittleman H, Farah P, Ondracek A, Chen Y, Wolinsky Y, *et al*. CBTRUS statistical report: Primary brain and central nervous system tumors diagnosed in the United States in 2006–2010. Neuro-oncology. 2013; 15: ii1–ii56.

[3] De Boeck A, Ahn BY, D'Mello C, Lun X, Menon SV, Alshehri MM, *et al*. Glioma-derived IL-33 orchestrates an inflammatory

Journal of
BIOLOGICAL REGULATORS
and Homeostatic Agents

brain tumor microenvironment that accelerates glioma progression. Nature Communications. 2020; 11: 4997.

[4] Berghoff AS, Kiesel B, Widhalm G, Wilhelm D, Rajky O, Kurscheid S, *et al*. Correlation of immune phenotype with IDH mutation in diffuse glioma. Neuro-oncology. 2017; 19: 1460–1468.

[5] Aldape K, Brindle KM, Chesler L, Chopra R, Gajjar A, Gilbert MR, *et al*. Challenges to curing primary brain tumours. Nature Reviews. Clinical Oncology. 2019; 16: 509–520.

[6] Zhao D, Zhang H, Uyar R, Hossain JA, Miletic H, Tonn JC, *et al*. Comparing Tumor Cell Invasion and Myeloid Cell Composition in Compatible Primary and Relapsing Glioblastoma. Cancers. 2021; 13: 3636.

[7] Cerami E, Gao J, Dogrusoz U, Gross BE, Sumer SO, Aksoy BA, *et al*. The cBio cancer genomics portal: an open platform for exploring multidimensional cancer genomics data. Cancer Discovery. 2012; 2: 401–404.

[8] Colaprico A, Silva TC, Olsen C, Garofano L, Cava C, Garolini D, *et al*. TCGAbiolinks: an R/Bioconductor package for integrative analysis of TCGA data. Nucleic Acids Research. 2016; 44: e71.

[9] Leek JT, Johnson WE, Parker HS, Jaffe AE, Storey JD. The sva package for removing batch effects and other unwanted variation in high-throughput experiments. Bioinformatics (Oxford, England). 2012; 28: 882–883.

[10] Iglesia MD, Vincent BG, Parker JS, Hoadley KA, Carey LA, Perou CM, *et al*. Prognostic B-cell signatures using mRNA-seq in patients with subtype-specific breast and ovarian cancer. Clinical Cancer Research: an Official Journal of the American Association for Cancer Research. 2014; 20: 3818–3829.

[11] Charoentong P, Finotello F, Angelova M, Mayer C, Efremova M, Rieder D, *et al*. Pan-cancer Immunogenomic Analyses Reveal Genotype-Immunophenotype Relationships and Predictors of Response to Checkpoint Blockade. Cell Reports. 2017; 18: 248–262.

[12] Newman AM, Liu CL, Green MR, Gentles AJ, Feng W, Xu Y, *et al*. Robust enumeration of cell subsets from tissue expression profiles. Nature Methods. 2015; 12: 453–457.

[13] Broz ML, Binnewies M, Boldajipour B, Nelson AE, Pollack JL, Erle DJ, *et al*. Dissecting the tumor myeloid compartment reveals rare activating antigen-presenting cells critical for T cell immunity. Cancer Cell. 2014; 26: 638–652.

[14] Teschendorff AE, Gomez S, Arenas A, El-Ashry D, Schmidt M, Gehrmann M, *et al*. Improved prognostic classification of breast cancer defined by antagonistic activation patterns of immune response pathway modules. BMC Cancer. 2010; 10: 604.

[15] Palmer C, Diehn M, Alizadeh AA, Brown PO. Cell-type specific gene expression profiles of leukocytes in human peripheral blood. BMC Genomics. 2006; 7: 115.

[16] Fan C, Prat A, Parker JS, Liu Y, Carey LA, Troester MA, *et al*. Building prognostic models for breast cancer patients using clinical variables and hundreds of gene expression signatures. BMC Medical Genomics. 2011; 4: 3.

[17] Rody A, Holtrich U, Pusztai L, Liedtke C, Gaetje R, Ruckhaeberle E, *et al*. T-cell metagene predicts a favorable prognosis in estrogen receptor-negative and HER2-positive breast cancers. Breast Cancer Research: BCR. 2009; 11: R15.

[18] Hänzelmann S, Castelo R, Guinney J. GSVA: gene set variation analysis for microarray and RNA-seq data. BMC Bioinformatics. 2013; 14: 7.

[19] Yoshihara K, Shahmoradgoli M, Martínez E, Vegesna R, Kim H, Torres-Garcia W, *et al*. Inferring tumour purity and stromal and immune cell admixture from expression data. Nature Communications. 2013; 4: 2612.

[20] Jiang P, Gu S, Pan D, Fu J, Sahu A, Hu X, *et al*. Signatures of T cell dysfunction and exclusion predict cancer immunotherapy response. Nature Medicine. 2018; 24: 1550–1558.

[21] Wang Z, Wang Y, Yang T, Xing H, Wang Y, Gao L, *et al*. Machine learning revealed stemness features and a novel stemness-based classification with appealing implications in discriminating the prognosis, immunotherapy and temozolomide responses of 906 glioblastoma patients. Briefings in Bioinformatics. 2021; 22: bbab032.

[22] Ritchie ME, Phipson B, Wu D, Hu Y, Law CW, Shi W, *et al*. limma powers differential expression analyses for RNA-sequencing and microarray studies. Nucleic Acids Research. 2015; 43: e47.

[23] Yu G, Wang LG, Han Y, He QY. clusterProfiler: An R package for comparing biological themes among gene clusters. Omics: A Journal of Integrative Biology. 2012; 16: 284–287.

[24] Mermel CH, Schumacher SE, Hill B, Meyerson ML, Beroukhim R, Getz G. GISTIC2.0 facilitates sensitive and confident localization of the targets of focal somatic copy-number alteration in human cancers. Genome Biology. 2011; 12: R41.

[25] Mayakonda A, Lin DC, Assenov Y, Plass C, Koeffler HP. Maftools: efficient and comprehensive analysis of somatic variants in cancer. Genome Research. 2018; 28: 1747–1756.

[26] Robin X, Turck N, Hainard A, Tiberti N, Lisacek F, Sanchez JC, *et al*. pROC: an open-source package for R and S+ to analyze and compare ROC curves. BMC Bioinformatics. 2011; 12: 77.

[27] Maccari M, Baek C, Caccese M, Mandruzzato S, Fiorentino A, Internò V, *et al*. Present and Future of Immunotherapy in Patients With Glioblastoma: Limitations and Opportunities. The Oncologist. 2023; oyad321.

[28] Yang Y, Fu X, Liu R, Yan L, Yang Y. Exploring the prognostic value of HK3 and its association with immune infiltration in glioblastoma multiforme. Frontiers in Genetics. 2023; 13: 1033572.

[29] Zhang M, Chen H, Liang B, Wang X, Gu N, Xue F, *et al*. Prognostic Value of mRNAsi/Corrected mRNAsi Calculated by the One-Class Logistic Regression Machine-Learning Algorithm in Glioblastoma Within Multiple Datasets. Frontiers in Molecular Biosciences. 2021; 8: 777921.

[30] Knijnenburg TA, Wang L, Zimmermann MT, Chambwe N, Gao GF, Cherniack AD, *et al*. Genomic and molecular landscape of DNA damage repair deficiency across the cancer genome atlas. Cell Reports. 2018; 23: 239–254. e6.

[31] Kurdi M, Butt NS, Baeesa S, Alghamdi B, Maghrabi Y, Bardeesi A, *et al*. Prognostic value of TP53 expression and MGMT methylation in glioblastoma patients treated with temozolomide combined with other chemotherapies. Journal of Neuro-oncology. 2021; 152: 541–549.